Laser Patterning of Epitaxial Graphene for Schottky Junction Photodetectors

Ram Sevak Singh,[†] Venkatram Nalla,[†] Wei Chen, Andrew Thye Shen Wee,[*] and Wei Ji[*]

Department of Physics, National University of Singapore, Singapore 117542, Singapore. [†]These authors contributed equally to this work.

ABSTRACT Large-area patterning of epitaxial graphene for Schottky junction photodetectors has been demonstrated with a simple laser irradiation method. In this method, semimetal—semiconductor Schottky junctions are created in a controllable pattern between epitaxial graphene (EG) and laser-modified epitaxial graphene (LEG). The zero-biased EG-LEG-EG photodetector exhibits a nanosecond and wavelength-independent photoresponse in a broad-band spectrum from ultraviolet (200 nm) through visible to infrared light (1064 nm), distinctively different from conventional photon detectors. An efficient external photoresponsivity (or efficiency) of ~0.1 $A \cdot W^{-1}$ is achieved with a biased interdigitated EG-LEG-EG photodetector. The fabrication method presented here opens a viable route to carbon optoelectronics for a fast and highly efficient photoconductive detector.

KEYWORDS: laser patterning · laser-modified epitaxial graphene · Schottky junction · photoconductive detector · scanning tunneling microscopy · Raman spectroscopy

Graphene, a two-dimensional hexagonal network of carbon atoms, is an emerging material for electronics and optoelectronics due to its exotic physical properties such as room-temperature quantum Hall effect, massless Dirac fermions, ballistic transport, and optical behavior.[1−3] The recent report[4] on the large-area production of epitaxial graphene (EG) by annealing of silicon carbide (SiC) stimulated a great deal of interest as it is compatible with industrial large-scale processing techniques. Transport measurements on EG showed high carrier mobilities (up to 25 000 $cm^2/V \cdot s$) and long phase coherence lengths, thereby making EG a promising candidate for low power consumption and fast electronic devices.[5] Carrier multiplication was also found to be a dominant phenomenon in graphene,[6,7] which could be utilized to enhance the conversion efficiency of solar cells.

However, many technical challenges remain. One challenge is the large-area patterning of EG *via* lithography which is compatible with current silicon-based fabrication technology. The other challenge is the development of a simple, low-cost technique for the making of p—n junctions or Schottky junctions, the key component in electronic and optoelectronic devices. Here, we report a simple technique for the large-scale patterning of Schottky junction within few-layer EG.

Graphene can be oxidized. For example, by the addition of oxidizing agents, it was converted to graphene oxide (GO) *via* a photochemical method,[8] or simply heating graphene in ambient turned graphene into GO.[9] Conversely, laser direct writing/exposing methods were employed by several research groups to reduce GO to graphene.[10−12] Wu and his co-workers[13] demonstrated that a Schottky junction was created if both EG and e-beam-modified GO were brought together in contact with each other. In this case, a semimetal—semiconductor Schottky junction was formed as EG was semimetallic,[10−12] and e-beam-modified GO showed semiconducting behavior.[13] However, their fabrication technique involves time-consuming processes with the limited controllability and lack of scalability. The laser patterning method presented here enables ones to modify EG locally to have semiconductor properties, thereby achieving a large-area patterning of a semimetal—semiconductor Schottky junction. This method would also allow a scaling beyond 2 in. SiC wafers currently available as well as integration with CMOS electronics. With this simple method, we demonstrate Schottky junction photoconductive detectors which offer advantages as follows. (1) Internal (built-in) electric fields, responsible for the separation of photogenerated charge carriers (electrons or holes), were found to be present in narrow regions (~0.2 μm) adjacent to the electrode—graphene interfaces in graphene field-effect transistor (FET) photodetectors.[14] In our device, the width of internal field is as large as ~400 μm, thereby enhancing the capability of electron—hole separation in a considerable amount and leading to a great efficiency of conversion from light to photocurrent. (2) Previously reported graphene- or GO-based devices[15,16] showed microsecond photoconductive decays, but our zero-biased devices

* Address correspondence to phyjiwei@nus.edu.sg, phyweets@nus.edu.sg.

Received for review May 13, 2011 and accepted June 24, 2011.

Published online June 24, 2011
10.1021/nn201757j

© 2011 American Chemical Society

exhibit nanosecond recovery times. (3) The most important feature is that the photoresponse of our devices is independent of light wavelength from ultraviolet (200 nm) through visible to infrared (1064 nm), a unique optical phenomenon only manifested itself in graphene as an active photosensor.

RESULTS AND DISCUSSION

To demonstrate the laser patterning method, we first prepared few-layer epitaxial graphene (EG) on the Si face of SiC substrates by thermal desorption of silicon at high temperatures in ultrahigh vacuum (UHV).[17−19] The preparation of few-layer EG was monitored by scanning tunneling microscopy (STM), as shown in Figure 1. A 100 nm thick layer of gold (Au) was thermally evaporated on them.

The laser patterning for single-line structures, as illustrated in Figure 2a, was carried out by the following two steps. First, the Au-coated sample was exposed to cylindrically focused laser pulses (1 mm × 3 mm). To evaporate a part of the Au film in the focused area, the exposure to 10 laser pulses (1.5 mJ per pulse, or fluence of 0.05 J cm^{-2}) was required. After the evaporation, the Au coating was split to two parts, used as two electrodes in photocurrent measurements described later. Second, it was irradiated with more laser pulses at the same energy, turning EG to laser-modified epitaxial graphene (LEG) with the degree of conversion depending on the number of laser pulses. The two steps were monitored *in situ* with a digital oscilloscope by collecting transient photocurrents in a short circuit of the two Au electrodes (the supporting video is also available as Supporting Information). Conversion from EG to LEG and formation of EG-LEG junction were confirmed by the transient photocurrent measurement in the second step, where the laser-induced photocurrent was enhanced drastically (within 60 laser pulses) and then clamped at a saturated level after complete conversion of EG. With this method, a 1 mm × 3 mm rectangular area (Figure 2a and Figure 3a) was created and two junctions (EG-LEG and LEG-EG) were found at the left and right edge, respectively. The same method was used to pattern the HOPG sample for comparison, but no photocurrent was observed with the laser pulse energy up to 4 mJ (or fluence up to 0.2 J cm^{-2}).

Both EG (unexposed to laser radiation) and LEG were investigated by Raman spectroscopy. The G-band in the Raman spectra of graphene is related to phonon vibrations in sp^2-bonded carbon materials, while the D-band is the signature for disorder induced by phonon scattering at defect sites and impurity.[18,20] The spectra in Figure 2c were obtained from the patterned areas using 514 nm excitation wavelength at room temperature and ambient environment. The spectrum in Figure 2c (iii) shows a broader G-band and intense D-band, similar to the two characteristic peaks of GO (or reduced GO).[21,22] Therefore, it is believed that LEG consists of GO or reduced GO (and detailed analyses can be found in Figure S4 of the Supporting Information). It was also observed that, once the conversion was complete, there was no increase in the transient photocurrent even after exposure to higher laser pulse energy in the range from 1.5 to 4 mJ. As a comparison, Figure 2c (ii) displays the spectrum recorded from the HOPG exposed to 4 mJ laser pulses, and the HOPG sample exposed to 1.5 mJ pulse energy showed no photoresponse. At pulse energies greater than 4.5 mJ, the occurrence of laser-induced damage was observed on the EG or HOPG. More details can be found in Supporting Information.

The mechanism of converting EG to LEG (GO or reduced GO) can be understood as a laser-induced oxidation/reduction process. The absorption of intense laser energy by EG gives rise to an increase in the temperature in the exposed area/volume, which in turn oxidizes EG itself in ambient environment by absorbing oxygen in the air. The laser-induced rise in the temperature of a material is proportional to the laser fluence (F), as given by the following equation[23]

$$\Delta T = \frac{B\eta F[1 - \exp(-\alpha d)]}{\rho CV} \quad (1)$$

where B is the exposed area of the material, η is the efficiency of conversion from the absorbed light energy into heat, ρ is the density of the material, C is the specific heat of the material, d is the material thickness, and V is the exposed volume. With $F = 0.05$ J cm^{-2}, an optical absorbance of bilayer EG = $[1 - \exp(-\alpha d)] \approx 0.05$ and an assumption of $\eta = 100\%$, we calculate ΔT in the range of 450−600 °C, for such high temperatures were sufficient for the oxidation/reduction.[24,25]

To gain more insights, we conducted position-dependent photocurrent scans. The 7 ns laser pulses were focused by a focusing lens onto the above-described device with a circular spot diameter of ~200 μm. Figure 3a displays both optical image and Raman spectra obtained from different locations on the device. Evidently, in the region near the Au electrode (the dashed line in Figure 3a), EG is unconverted due to lower laser irradiation resulting from the edge in the Gaussian spatial profile of laser pulses;the central region (blue in Figure 3a) is fully converted to LEG, supported by the Raman spectra (Figure 3a). Thus, two Schottky junctions are produced in a back-to-back format, as shown by a schematic in Figure 3b. Figure 3c shows that the photocurrent is maximized (absolute value) at ±0.5 mm from the center, with polarity consistent with the observation from graphene−metal junction devices.[14,26] The formation of two Schottky barriers manifests itself in the measured signals where the maximum indicates the maximum built-in field. If the effective internal field width is defined as the full width of half-maximum (absolute value) in the photocurrent measurement, a width

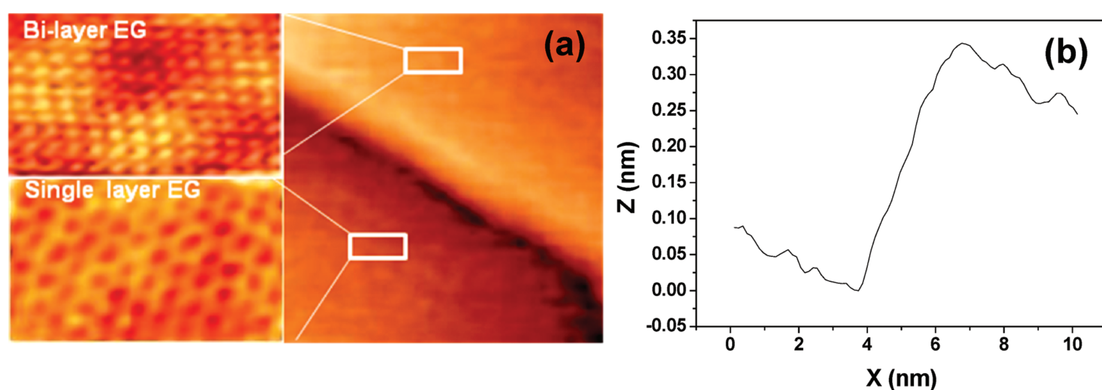

Figure 1. STM images of 1–2 layer epitaxial graphene (EG) on semi-insulating 4H-SiC (0001): (a) 40 × 40 nm^2 STM image (V_{tip} = 0.81 V) showing two regions (single-layer and bilayer EG) separated by a step of 0.35 nm. Atomically resolved STM images (left side) of single- and bilayer EG (V_{tip} = 0.16 V) taken from the highlighted area. (b) Line profile across the step extracted from the STM image in (a).

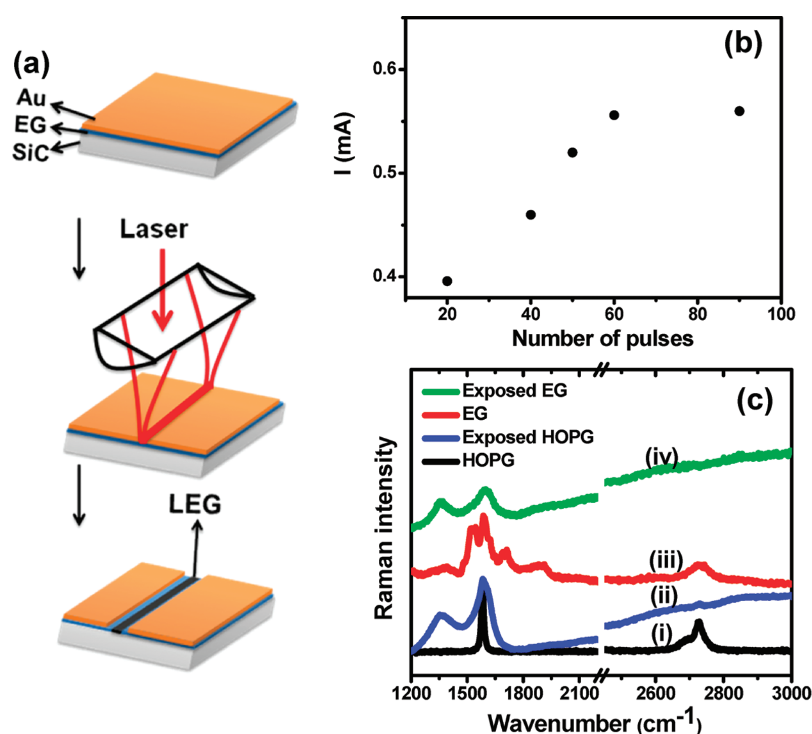

Figure 2. (a) Schematic diagram showing both evaporation of a rectangular part of the Au film and conversion from EG to LEG. (b) *In situ* monitoring of transient photocurrent as a function of laser pulse number after the evaporation of Au film. (c) Raman spectra recorded after the evaporation of Au film: (i) HOPG unexposed and (ii) HOPG exposed to 100 laser pulses; and (iii) EG unexposed and (iv) EG exposed to 100 laser pulses.

of ~400 μm can be determined from Figure 3c. It is in this region (400 μm × 3 mm) where the separation of photogenerated pairs of charge carriers (electrons or holes) occurs and, subsequently, separated charge carriers are collected by the Au electrode as the measured photocurrent.

The junction formation, coupled with high mobility of graphene, enables photogenerated charge carriers to be separated and extracted efficiently by the Au electrodes, thereby shortening the photocurrent recovery time, as supported by our transient measurements. The measured photocurrent decay times depend on the location, as shown in Figure 3d; the further away from the Au electrodes, the longer the decay times. The discontinuity in the decay time implies that the photodynamic mechanism in the LEG region be entirely different from the EG-LEG junction. No photocurrent was observed when the measurement was conducted on the central LEG region or the Au film.

Furthermore, photoconductive responses of the EG-LEG-EG junction depend on the excitation energy. As the excitation pulse energy grows, the photocurrent tends to saturate, as shown in Figure 4. The saturation

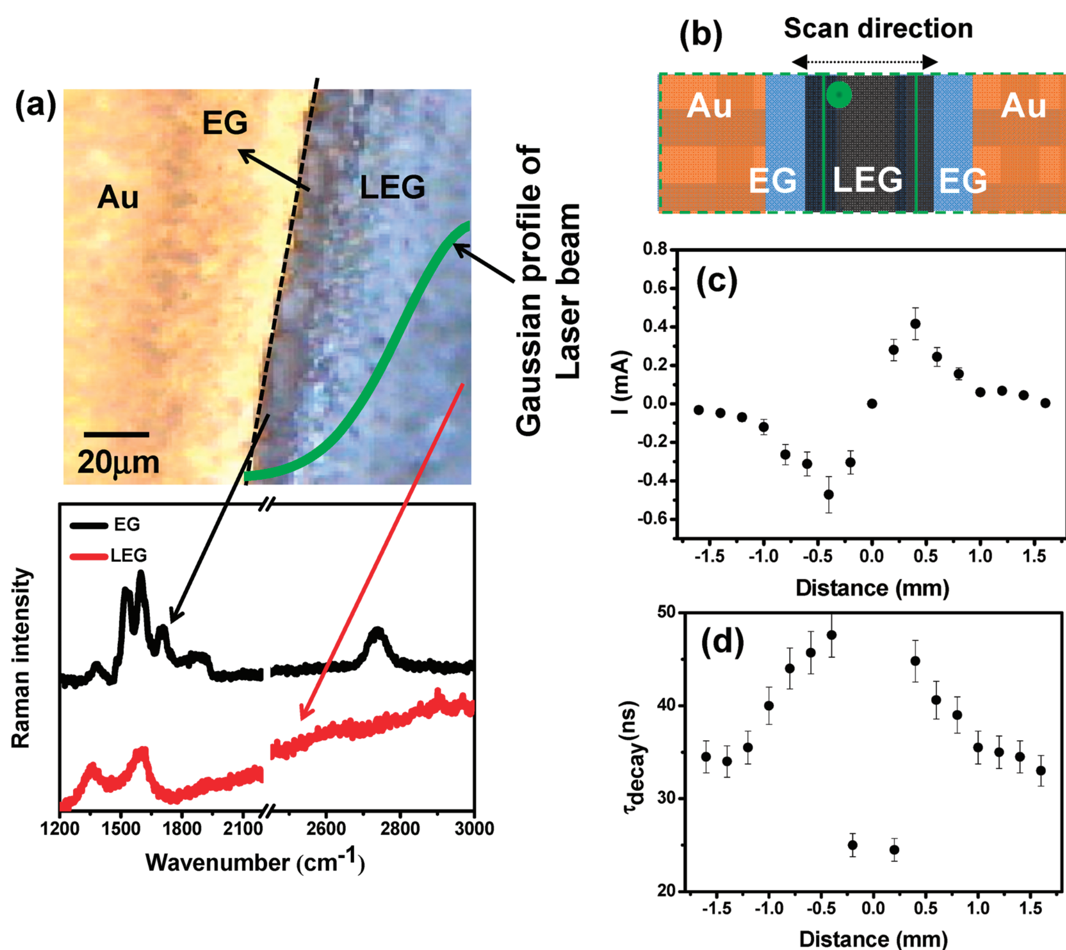

Figure 3. (a) Optical image and Raman spectra measured from the unconverted EG (black) and LEG (red) region. (b) Schematic of photocurrent line scanning across the EG-LEG-EG junction. (c) Maximal transient photocurrent and (d) photocurrent decay time as a function of the distance from the center when illuminated by laser pulses at 50 μJ per pulse. The green line in (a) represents the spatial profile of the laser pulse used for conversion from EG to LEG. The green spot in (b) represents the area illuminated for the photocurrent measurement.

could be a result of saturation of light absorption.[27] Photothermoelectric effect across the interface between two different materials due to high photoexcited carrier density could also account for the saturation of photocurrent.[28] Panels a and b of Figure 4 display the laser-pulse energy-dependent temporal profiles of photocurrent pulses excited at 1064 and 532 nm, respectively, which fit well with the single exponential decay time and the rising time of ~7 ns. As shown in Figure 4d, the decay becomes slower with the increase of excitation pulse energy. At higher laser excitation, more carriers are photogenerated, resulting in slower decays due to carrier phonon scattering in EG, LEG, or substrates.[27,29] The photocurrent decay times are faster at 532 nm, as compared with 1064 nm (see Figure 4d). This is consistent with avalanche photodiodes, whereby exciting with higher energy photons results in an increase in the kinetic energy of photocarriers, giving rise to shorter decay times.[30,31]

Figure 4c also shows that the same magnitude of photocurrent is observed for the two wavelengths at the same pulse energy, indicating that the photoresponsivity is independent of light wavelength. Such wavelength independence indicates that EG plays an important role in the photogeneration, consistent with the light-wavelength-independent absorption characteristic of graphene. This is completely different from conventional semiconductor photon detectors whose optical responses strongly depend on light wavelength.

The wavelength independence was further validated by our DC photocurrent measurement in the spectral range from 200 to 1000 nm. From the measurement in Figure 5, the internal photoresponsivity (or efficiency) defined below is found to be ~3.3 mA W^{-1}.

$$R(\lambda) = \frac{I_{ph}}{[1 - \exp(-\alpha d)]BI(\lambda)} \quad (2)$$

where I_{ph} is the collected photocurrent, B is the illuminated EG-LEG surface area (0.4 mm × 2 mm), and $I(\lambda)$ is the intensity spectrum of the incident light. The measured spectral responsivity shows a uniform response (within the error of 10%) covering from ultraviolet (200 nm) through visible to infrared (1000 nm) wavelengths. Figure 5 also shows the noise level measured

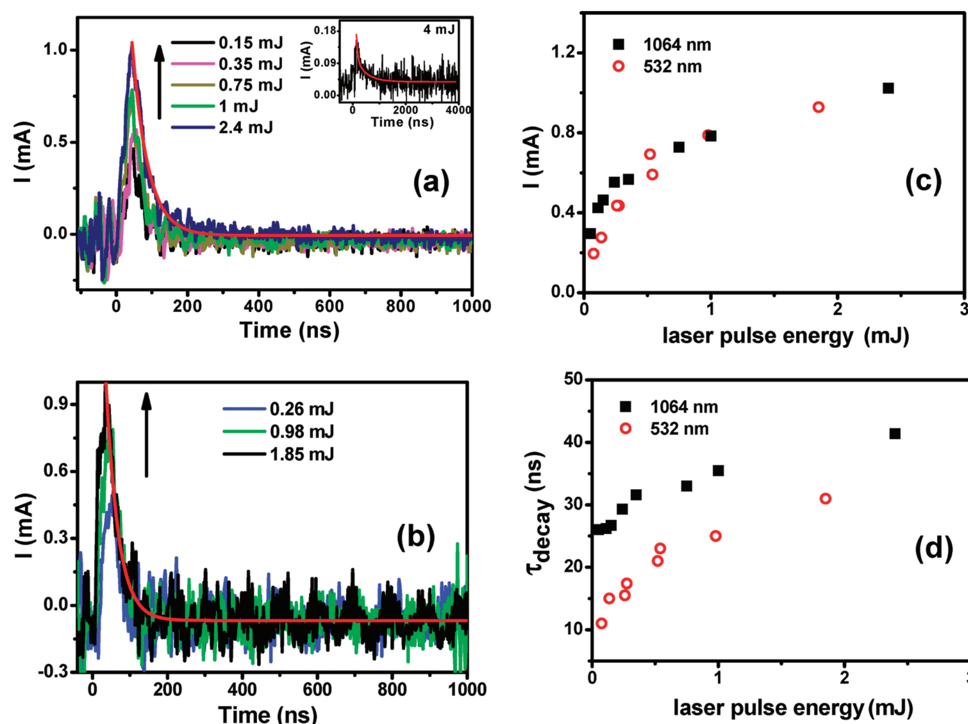

Figure 4. Temporal photocurrent profiles of the EG-LEG-EG junction when one junction is excited at (a) 1064 nm and (b) 532 nm laser pulses. The inset in (a) shows the transient photocurrent profile of the HOPG sample at 1064 nm. The red line is a single exponential fit. Photocurrent maxima (c) and decay times (d) excited at 532 and 1064 nm as a function of laser pulse energy.

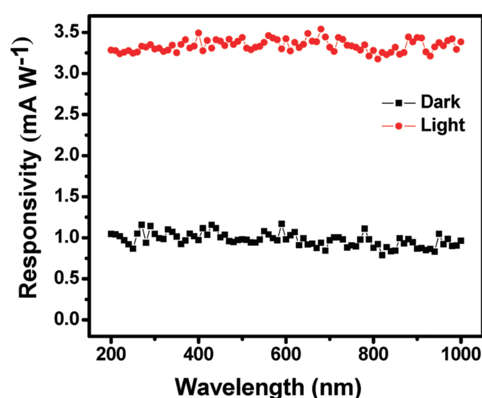

Figure 5. Internal spectral responsivity of the EG-LEG-EG junction device under zero bias.

under dark, the origin of which is still unclear and more investigations are required. Such a unique response makes the EG-LEG-EG photodetector versatile for many applications. It should be mentioned that an external photoresponsivity of 6.1 mA W^{-1} in a biased graphene photoconductor was observed at 1.55 μm.[14] As such, we conclude that graphene-based photoconductive devices are not only excellent visible–infrared sensors, but they are also superior ultraviolet (UV) detectors.

We also fabricated an interdigitated EG-LEG-EG device, and the top view of the device is shown in the inset of Figure 6. In this device, the structure consists of several vertical and horizontal lines. The length of each vertical line was controlled by the size of a rectangular aperture placed in front of the cylindrical lens. The horizontal line was made by rotating the device 90° around the laser beam. The $I-V$ curve of the device under dark exhibits strong semiconducting behavior, as shown in Figure 6a. The photoresponse was measured when the entire surface of the inset in Figure 6a was illuminated with the same solar simulator. From Figure 6a, an external photoresponsivity (or efficiency) of 0.1 A/W (after the dark current was deducted) is achieved at a bias voltage of −10 V.

The $I-V$ curves in Figure 6a can be explained by a commonly used circuit model in which two opposing Schottky diodes are connected in a series, as shown in Figure 6b. The corresponding band diagram and photoexcitation are displayed in Figure 6c. The nonlinear $I-V$ characteristic of each Schottky junction can be expressed by the thermoionic emission model.[32] The total current (I) and bias voltage (V) are given by

$$I = -I_{P1} + A_1 A^* T^2 e^{-\varphi_1/kT}(e^{qV_1/nkT} - 1) + I_{P2} - A_2 A^* T^2 e^{-\varphi_2/kT}(e^{-qV_2/nkT} - 1) \quad (3)$$

$$V = V_1 + V_2 + V_{LEG} \quad (4)$$

where A^* is the effective Richardson constant, n is the diode ideality factor, q is the electron charge; k is the Boltzmann constant, and T (=297 K) is the temperature. I_{P1}, I_{P2} are the photocurrents, A_1, A_2 are the contact areas between EG and LEG, V_1, V_2 are the voltage drops,

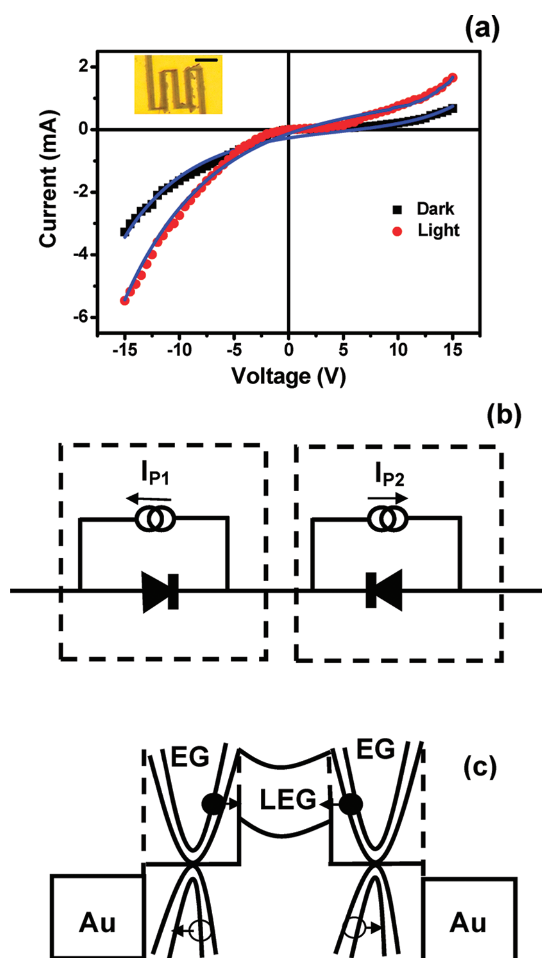

Figure 6. $I-V$ characteristics (filled squares) of the interdigitated device with (red) and without (black) white light illumination at 100 mW/cm^2. The solid curves (blue) are the modeling. The inset shows the top view of the device with the scale bar = 1 mm. The asymmetry with respect to the bias voltage is primarily due to the dissimilarity of the two junctions.

and φ_1, φ_2 are the Schottky barrier heights of diode 1 and diode 2, respectively. V_{LEG} is the voltage drop across the LEG region. The fittings to both dark and illuminated $I-V$ curves were achieved at $\varphi_1 = 0.75$ eV, $\varphi_2 = 0.70$ eV, $I_{P1} = I_{P2} = 0$ for dark, and $I_{P1} \approx 13$ mA, $I_{P2} \approx 16$ mA under light illumination. By considering $A_1 = A_2$ ($\approx$thickness of EG $\times$ length of Schottky junction $\approx 9 \times 10^{-8}$ cm^2) and $n = 2$, the effective Richardson constant A^* extracted from the best fit is 8850 A cm^{-2} K^{-2}, comparable to the reported constant for the Pt–Si Schottky junction.[33] The two Schottky barrier heights (φ_1 = 0.75 eV, φ_2 = 0.70 eV) are close to the reported value of 0.7 eV by Wu *et al.*,[13] indicating that the LEG is a semiconductor. In the curve fitting, voltage drops were floated, the best fit was achieved at $V_1 = 0.07 \times V$, $V_2 = 0.08 \times V$, revealing that 85% of the total bias voltage is dropped on the LEG region as $V_{LEG} = 0.85 \times V$. This provides a practical means to reduce the operating bias voltage by designing a narrower width of the LEG region.

The $I-V$ characteristics of the above device suggest that LEG should be a semiconductor. To further support it, we carried out an additional experiment: the total area of a 3 mm $\times$ 10 mm EG sample was modified to LEG. Then, we measured its infrared absorption spectrum, from which we determined that LEG indeed shows semiconducting properties, with a band gap of ~0.63 eV. (More details can be found in Figure S8 of the Supporting Information.) The calculated lower limit to the mobility of the LEG is 650 cm^2/V·s at room temperature, which is comparable to the previous reports on e-beam-modified graphene oxide.[13]

In summary, we have demonstrated the fabrication of a large-area of EG-LEG-EG Schottky junction device on SiC substrates with a simple laser irradiation method. These zero-biased junction devices show nanosecond photoresponses, making them promising for high-speed applications. More importantly, the devices exhibit a uniform broad-band (200–1064 nm) photoresponse, demonstrating that the EG-LEG-EG Schottky junction devices are not only excellent visible and infrared sensors but also superior UV detectors, which is distinctively different from conventional semiconductor photon detectors whose photoresponse strongly depends on light wavelengths. An efficient external photoresponsivity (or efficiency) of ~0.1 A·W^{-1} is achieved with a biased interdigitated EG-LEG-EG photodetector. The fabrication method presented here opens a viable route to carbon optoelectronics for fast and highly efficient photoconductive detectors.

EXPERIMENTAL SECTION

Materials. Two types of materials were used in this study, epitaxial graphene (EG) and highly oriented pyrolytic graphite (HOPG). The HOPG substrate (purchased from Mateck GmbH Company) was well cleaved to flatten the surface prior to using it as a sample for devices. EG films (1–2 layers) were prepared by annealing chemically etched (10% HF solution) high-purity, semi-insulating 4H-SiC (0001) (resistivity $\geq 10^5$ Ω·cm and thickness = 0.37 mm, CREE Research Inc.) in ultrahigh vacuum (UHV) above 1100 °C.[17–19]

Laser Patterning. Next, 1064 nm wavelength, 7 ns duration, and 10 Hz repetition rate laser pulses were generated by a Nd:YAG laser (Spectra Physics Quanta Ray) and were focused with cylindrical lens for laser patterning.

Transient Photocurrent Measurements. EG-LEG-EG Schottky junction devices were excited with 1064 and 532 nm wavelength, 7 ns duration, and 10 Hz repetition rate laser pulses, generated by the Nd:YAG laser (Spectra Physics Quanta Ray). The temporal photocurrent profiles were collected with a digital oscilloscope (Tektronix TDS 380, 50 ohm terminated, 400 MHz bandwidth); the positive and negative terminals of the oscilloscope were directly connected to the two Au electrodes, respectively. Optical neutral density filters were employed to control the laser pulse energy. A laser power meter (Laser probe, Rj-760)

was used to measure the average power of the laser pulses. All of the transient photocurrent measurements were carried out in air at room temperature without any biased voltage.

Wavelength-Dependent DC Photocurrent Measurement. DC photocurrent measurement in the spectral range from 200 to 1000 nm was carried out using a solar simulator (AM 1.5G light source) produced by a Newport 300 W xenon light source and controlled by a Newport Digital Exposure Controller, which simulated the solar light through an AM 1.5G sunlight filter. The continuous wave (cw) white light propagated through a monochromator and was then focused onto one junction of the EG-LEG-EG device with intensity calibrated to 100 mW cm^{-2} at each wavelength.

Acknowledgment. The authors would like to acknowledge the Faculty of Science, National University of Singapore, and the NRF CRP Grant R-143-000-360-281 for financial support.

Supporting Information Available: In situ photocurrent monitoring during the fabrication of single-line EG-LEG-EG junction device (video), detected signals of laser pulses over one second, pulse-energy-dependent photocurrent temporal profiles, Raman spectra of modified HOPG at different pulse energies, detailed analyses on the Raman spectra of LEG, *I*−*V* characteristics of the single-line EG-LEG-EG junction device, AFM images of EG before and after modification with laser beams and optical absorption spectra of EG and LEG. This material is available free of charge *via* the Internet at http://pubs.acs.org.

REFERENCES AND NOTES

1. Novoselov, K. S.; Geim, A. K.; Morozov, S. V.; Jiang, D.; Zhang, Y.; Dubonos, S. V.; Grigorieva, I. V.; Firsov, A. A. Electric Field Effect in Atomically Thin Carbon Films. *Science* **2004**, *306*, 666–669.
2. Geim, A. K. Graphene: Status and Prospects. *Science* **2009**, *324*, 1530–1534.
3. Blake, P.; Brimicombe, P. D.; Nair, R. R.; Booth, T. J.; Jiang, D.; Schedin, F.; Ponomarenko, L. A.; Morozov, S. V.; Gleeson, H. F.; Hill, E. W.; *et al.* Graphene-Based Liquid Crystal Device. *Nano Lett.* **2008**, *8*, 1704–1708.
4. Berger, C.; Song, Z.; Li, T.; Li, X.; Ogbazghi, A. Y.; Feng, R.; Dai, Z.; Marchenkov, A. N.; Conrad, E. H.; First, P. N.; *et al.* Ultrathin Epitaxial Graphite: 2D Electron Gas Properties and a Route toward Graphene-Based Nanoelectronics. *J. Phys. Chem. B* **2004**, *108*, 19912–19916.
5. Bolotin, K. I.; Sikes, K. J.; Jiang, Z.; Klima, M.; Fudenberg, G.; Hone, J.; Kim, P.; Stormer, H. L. Ultrahigh Electron Mobility in Suspended Graphene. *Solid State Commun.* **2008**, *146*, 351–355.
6. McClain, J.; Schrier, J. Multiple Exciton Generation in Graphene Nanostructures. *J. Phys. Chem. C* **2010**, *114*, 14332–14338.
7. Winzer, T.; Knorr, A.; Malic, E. Carrier Multiplication in Graphene. *Nano Lett.* **2010**, *10*, 4839–4843.
8. Liu, H. T.; Ryu, S. M.; Chen, Z. Y.; Steigerwald, M. L.; Nuckolls, C.; Brus, L. E. Photochemical Reactivity of Graphene. *J. Am. Chem. Soc.* **2009**, *131*, 17099–17101.
9. Ryu, S.; Liu, L.; Berciaud, S.; Yu, Y.-J.; Liu, H.; Kim, P.; Flynn, G. W.; Brus, L. E. Atmospheric Oxygen Binding and Hole Doping in Deformed Graphene on a SiO_2 Substrate. *Nano Lett.* **2010**, *10*, 4944–4951.
10. Zhang, Y. L.; Guo, L.; Wei, S.; He, Y. Y.; Xia, H.; Chen, Q. D.; Sun, H. B.; Xiao, F. S. Direct Imprinting of Microcircuits on Graphene Oxides Film by Femtosecond Laser Reduction. *Nano Today* **2010**, *5*, 15–20.
11. Sokolov, D. A.; Shepperd, K. R.; Orlando, T. M. Formation of Graphene Features from Direct Laser-Induced Reduction of Graphite Oxide. *J. Phys. Chem. Lett.* **2010**, *1*, 2633–2636.
12. Abdelsayed, V.; Moussa, S.; Hassan, H. M.; Aluri, H. S.; Collinson, M. M.; El-Shall, M. S. Photothermal Deoxygenation of Graphite Oxide with Laser Excitation in Solution and Graphene-Aided Increase in Water Temperature. *J. Phys. Chem. Lett.* **2010**, *1*, 2804–2809.
13. Wu, X. S.; Sprinkle, M.; Li, X. B.; Ming, F.; Berger, C.; de Heer, W. A. Epitaxial-Graphene/Graphene-Oxide Junction: An Essential Step towards Epitaxial Graphene Electronics. *Phys. Rev. Lett.* **2008**, *101*, 026801.
14. Mueller, T.; Xia, F.; Avouris, P. Graphene Photodetectors for High-Speed Optical Communications. *Nat. Photonics* **2010**, *4*, 297–301.
15. Lv, X.; Huang, Y.; Liu, Z.; Tian, J.; Wang, Y.; Ma, Y.; Liang, J.; Fu, S.; Wan, X.; Chen, Y. Photoconductivity of Bulk-Film-Based Graphene Sheets. *Small* **2009**, *5*, 1682–1687.
16. Nalla, V.; Polavarapu, L.; Manga, K. K.; Goh, B. M.; Loh, K. P.; Xu, Q. H.; Ji, W. Transient Photoconductivity and Femtosecond Nonlinear Optical Properties of a Conjugated Polymer−Graphene Oxide Composite. *Nanotechnology* **2010**, *21*, 415203.
17. Ang, P. K.; Chen, W.; Wee, A. T. S.; Loh, K. P. Solution-Gated Epitaxial Graphene as pH Sensor. *J. Am. Chem. Soc.* **2008**, *130*, 14392–14393.
18. Chen, W.; Chen, S.; Qi, D. C.; Gao, X. Y.; Wee, A. T. S. Surface Transfer p-Type Doping of Epitaxial Graphene. *J. Am. Chem. Soc.* **2007**, *129*, 10418–10422.
19. Ni, Z. H.; Chen, W.; Fan, X. F.; Kuo, J. L.; Yu, T.; Wee, A. T. S.; Shen, Z. X. Raman Spectroscopy of Epitaxial Graphene on a SiC Substrate. *Phys. Rev. B* **2008**, *77*, 115416.
20. Ni, Z. H.; Fan, H. M.; Feng, Y. P.; Shen, Z. X.; Yang, B. J.; Wu, Y. H. Raman Spectroscopic Investigation of Carbon Nanowalls. *J. Chem. Phys.* **2006**, *124*, 204703.
21. Kudin, K. N.; Ozbas, B.; Schniepp, H. C.; Prud'homme, R. K.; Aksay, I. A.; Car, R. Raman Spectra of Graphite Oxide and Functionalized Graphene Sheets. *Nano Lett.* **2007**, *8*, 36–41.
22. Yang, D.; Velamakanni, A.; Bozoklu, G.; Park, S.; Stoller, M.; Piner, R. D.; Stankovich, S.; Jung, I.; Field, D. A.; Ventrice, C. A., Jr.; *et al.* Chemical Analysis of Graphene Oxide Films after Heat and Chemical Treatments by X-ray Photoelectron and Micro-Raman Spectroscopy. *Carbon* **2009**, *47*, 145–152.
23. Wang, N.; Yao, B. D.; Chan, Y. F.; Zhang, X. Y. Enhanced Photothermal Effect in Si Nanowires. *Nano Lett.* **2003**, *3*, 475–477.
24. Liu, L.; Ryu, S.; Tomasik, M. R.; Stolyarova, E.; Jung, N.; Hybertsen, M. S.; Steigerwald, M. L.; Brus, L. E.; Flynn, G. W. Graphene Oxidation: Thickness-Dependent Etching and Strong Chemical Doping. *Nano Lett.* **2008**, *8*, 1965–1970.
25. Ryu, S.; Han, M. Y.; Maultzsch, J.; Heinz, T. F.; Kim, P.; Steigerwald, M. L.; Brus, L. E. Reversible Basal Plane Hydrogenation of Graphene. *Nano Lett.* **2008**, *8*, 4597–4602.
26. Xia, F.; Mueller, T.; Golizadeh-Mojarad, R.; Freitag, M.; Lin, Y.-m.; Tsang, J.; Perebeinos, V.; Avouris, P. Photocurrent Imaging and Efficient Photon Detection in a Graphene Transistor. *Nano Lett.* **2009**, *9*, 1039–1044.
27. Mishchenko, E. G. Dynamic Conductivity in Graphene beyond Linear Response. *Phys. Rev. Lett.* **2009**, *103*, 246802.
28. Xu, X.; Gabor, N. M.; Alden, J. S.; van der Zande, A. M.; McEuen, P. L. Photo-Thermoelectric Effect at a Graphene Interface Junction. *Nano Lett.* **2010**, *10*, 562–566.
29. Xing, G.; Guo, H.; Zhang, X.; Sum, T. C.; Huan, C. H. A. The Physics of Ultrafast Saturable Absorption in Graphene. *Opt. Express* **2010**, *18*, 4564–4573.
30. Berndt, K.; Dürr, H.; Palme, D. Picosecond Phase Fluorometry and Color Delay Error. *Opt. Commun.* **1983**, *47*, 321–323.
31. Rayner, D. M.; McKinnon, A. E.; Szabo, A. G.; Hackett, P. A. Confidence in Fluorescence Lifetime Determinations: A Ratio Correction for the Photomultiplier Time Response with Wavelength. *Can. J. Chem.* **1976**, *54*, 3246–3259.
32. Sze, S. M.; Ng, K. K. *Physics of Semiconductor Devices*, 3rd ed.; John Wiley & Sons, Inc.: New York, 2007.
33. Toyama, N. Effective Richardson Constant of Sputtered Pt−Si Schottky Contacts. *J. Appl. Phys.* **1988**, *64*, 2515–2518.